FGL2-targeted T cells induced tumor-specific brain resident T_{RM} cells preventing glioblastoma recurrence

Qingnan Zhao
Shanghai Jiao Tong University School of Medicine
Ling-Yuan Kong
University of Texas MD Anderson Cancer Center
Shan Jiang
The University of Texas Health Science Center at Houston
Xiangjun Tian
The University of Texas MD Anderson Cancer Center
Jing Wang
UT M.D. Anderson Cancer Center https://orcid.org/0000-0002-5398-0802
Rintaro Hashizume
Northwestern University
Jiemiao Hu
The University of Texas MD Anderson Cancer Center https://orcid.org/0000-0002-5142-0641
Zhiliang Jia
The University of Texas MD Anderson Cancer Center
Natalie Fowlkes
The University of Texas MD Anderson Cancer Center https://orcid.org/0000-0002-7711-6031
Jun Yan
University of Texas MD Anderson Cancer Center
Xeuqing Xia
MD Anderson Cancer Center
Sofia Yi
The University of Texas MD Anderson Cancer Center
Long Dao
The University of Texas MD Anderson Cancer Center
David Masopust
University of Minnesota https://orcid.org/0000-0002-9440-3884
Hideho Okada
UCSF, USA https://orcid.org/0000-0003-0076-9920
Amy Heimberger

Northwestern University https://orcid.org/0000-0002-9970-8695

Shulin Li (SLi4@mdanderson.org)

The University of Texas MD Anderson Cancer Center https://orcid.org/0000-0001-5657-4183

Article

Keywords: T-αFGL2, glioblastoma, Tissue-resident memory T cells, CD69, CXCR3

Posted Date: May 11th, 2022

DOI: https://doi.org/10.21203/rs.3.rs-1632572/v1

Version of Record: A version of this preprint was published at Nature Communications on February 10th, 2023. See the published version at https://doi.org/10.1038/s41467-023-36430-2.

Abstract

Tissue-resident memory T cells (T_{RM}) specific to previously encountered pathogens have been characterized, but tumor-specific T_{RM} cells in brain have not been reported in the literature. We discovered that T cells armed with FGL2-blocking single-chain variable fragments (T-αFGL2) are able to induce tumor-specific $CD8^+T_{RM}$ cells, which prevent glioblastoma recurrence, a major obstacle in achieving long term survivors. These tumor-specific $CD8^+T_{RM}$ displayed a unique highly expanded T cell receptor repertoire distinct from that found in peripheral tissues. Notably, these $CD8^+T_{RM}$ cells could be transplanted into the brains of either immunocompetent or T cell deficient naïve mice, transforming them to become immune reactive to tumor cells. The mechanism study found T-αFGL2 therapy boosted $CD69^+CD8^+$ memory T cells population in tumor bearing brains, which depend on CXCL9/10-CXCR3 signaling. These findings are the first to show tumor-specific brain resident $CD8^+T_{RM}$ generation via adoptive cellular treatment and may have promising implications for cancer immunotherapy.

Significance Statement

1. T cells armed with FGL2-blocking single-chain variable fragments (T-αFGL2) were able to induce tumor-specific $CD8^+T_{RM}$ cells.
2. These tumor-specific $CD8^+T_{RM}$ cells are tumor reactive and transplantable.
3. The induced tumor-specific $CD69^+CD62L^-CD8^+T_{RM}$ cells, displayed a highly expanded T cell receptor repertoire.
4. CXCL9/10-CXCR3 signaling was associated with $CD69^+CD8^+T_{RM}$ induction.

Introduction

Memory T cells provide rapid and effective immune protection against a wide variety of antigens, including those from environmental substances and malignant tumors. Memory T cells consist of two major populations: non-recirculating resident memory T (T_{RM}) cells[1,2] and recirculating memory T cells[3]. recirculating memory T cellsinclude effector memory T (T_{EM}) cells, central memory T cells (T_{CM}), and migratory memory T cells. Research has shown that T_{RM} cells are more potent effectors than recirculating memory T cells[4–7]. T_{RM} cells, often bearing CD69 and the αEβ7 integrin (CD103), and null of CD62L, offer dominant immunity to localized infection[8]. CD103 binds to epithelial E-cadherin, while CD69 blocks cellular egress via inhibition of the function of Sphingosine-1-phosphate receptor-1 (S1PR1)[9], both help T_{RM} cells retain in peripheral tissues. CD62L is lymphoid homing molecule, which helps peripheral T cells homing to secondary lymphoid organs. To date, T_{RM} cells have been found in both barrier and non-barrier tissues, including the skins[10,11], brains[12], lungs[13–17], livers[18], and breasts[19], where they mediate long-lived protection against reinfection. However, how to induce T_{RM} cell formation in tumor-bearing tissues,

especially glioblastoma (GBM) with high fatality rate, thus leading to tumor contraction and recurrence prevention, has rarely been studied.

As a member of the fibrinogen-like protein family, fibrinogen-like protein 2 (FGL2) possesses prothrombinase activity and immune regulatory functions in both viral infection and cancer development. Accumulating evidence shows that FGL2 acts as an immunosuppressive regulator, suppressing B cell, T cell, and dendritic cell (DC) functions by binding to FcγRIIB and regulating adaptive immunity via Th1 and Th2 cytokines[20]. Our previously published data showed that overexpression of FGL2 correlates with upregulated expression of negative immune checkpoints, decreased granulocyte-macrophage colony-stimulating factor induced $CD103^+$ DC differentiation, faster glioma progression, and poor clinical outcome in brain malignancies[20–23].

An analysis of TCGA data found an inverse correlation between FGL2 expression and patient with GBM survival[22]; therefore, FGL2 may serve as an attractive target for brain tumor immunotherapy. Indeed, FGL2-specific polyclonal antibodies showed antitumor activity against GBM tumor cells in syngeneic mouse models[23]. However, owing to their poor blood-brain barrier penetration, the potential of FGL2-blocking antibodies to suppress brain tumor progression is limited.

Here, to improve the efficacy of an FGL2-blocking antibody in treating brain tumors, we performed adoptive cell infusion of T cells armed with an FGL2-blocking single-chain variable fragment (scFv). These T cells bearing FGL2-blocking scFv (T-αFGL2) showed superior potent anti-tumor effects compared with control T cells (T-Ctr) without causing obvious toxicity at the therapeutic dose. Importantly, the long-term mouse survivors in the T-αFGL2 treatment group formed tumor-specific brain-resident memory $CD8^+$T ($CD8^+T_{RM}$) cells that rejected rechallenged tumor cells in the brain. These $CD8^+T_{RM}$ cells are $CD69^+CD8^+$ T cells that display an expanded T cell receptor (TCR) repertoire. Of note, the $CD8^+T_{RM}$ cells can be transplanted into the brains of naïve mice to convert these naïve mice into $CD8^+T_{RM}$-bearing mice, enabling these mice to reject tumor cells upon rechallenge. We report that T-αFGL2 treatment boosted $CD69^+CD62L^-CD8^+$T cells population, and this effect was abolished when depleting either CXCR3 ligands CXCL9/10 or knockout of CXCR3 in the host mice, revealing an unanticipated novel link between CXCL9/10-CXCR3 signaling and tumor specific $CD8^+T_{RM}$ formation in brains.

Results

T-αFGL2 treatment has limited antitumor cytotoxic T lymphocyte activity *in vitro*

To obtain superior FGL2 specific monoclonal antibodies (mAbs), we selected 75 clones of FGL2 mAbs through 3 independent hybridoma fusion and via an ELISA-based mouse FGL2 (mFGL2) binding assay (Supplementary Fig. 1a). 13 out of 75 clones showed strong binding activity to mFGL2 but not to his-tag. Human FGL2 (huFGL2) was then used to select mAbs that show bi-species binding reactivity (Supplementary Fig. 1b), and mouse FGL2 binding clone #4 also showed high binding affinity to human

FGL2 (Supplementary Fig. 1a, 1b). Additionally, clone #4 showed the most linear association between binding capacity and dilution (Supplementary Fig. 1c). Western blotting, immunofluorescence staining, and ELISA assay further validated the binding activity of FGL2 mAb-clone #4 to both mouse and human FGL2 (Supplementary Fig. 1d-1f). To further test the effect of FGL2 blocking scFv, lentiviral constructs derived from FGL2 mAb-clone #4 were generated to arm T cells (Fig 1a). This construct contained scFv domains that aimed at recognizing and binding FGL2 (Fig 1a). To ensure that FGL2 scFv was expressed on the surface of T cells with the ability of movement, an EGFR-transmembrane (TM) domain was linked to the FGL2 scFv by a P2A linker (Fig 1a, 1b). The expression of FGL2 scFv on the T cell membrane was validated by the staining of the His tag domain (Fig 1c). The transduction efficiency of the activated mouse T cells was consistent and in the range of 15% to 25% (Fig 1c). To verify that T-αFGL2 cells can directly bind FGL2, we have established a microfluidics chip binding assay. As the data shown in Supplementary Fig.1g, T-αFGL2 cells can directly bind the FGL2 that is anchored on the chip via biotin-streptavidin covalent bond. The antitumor cytotoxic T lymphocyte activity of FGL2-scFv–armed T cells (T-αFGL2) against FGL2-expressing DBT cells, a mouse GBM cell line, was evaluated by measuring proportion of tumor cells, and granzyme B, interferon γ (IFNγ), and tumor necrosis factor α (TNFα) positive T cells (Fig. 1d). T-αFGL2 cells expressed higher granzyme B levels than did T cells transfected with a control construct (T-Ctr) when cocultured with DBT cells at an effector-to-target ratio of 1:1. However, no significant difference was found in the proportion of tumor cells when cocultured with T-αFGL2 and T-Ctr cells, and T-αFGL2 and T-Ctr cells had comparable levels of IFNγ and TNFα, suggesting that T-αFGL2 may have limited direct tumor cell killing activity effects *in vitro*.

T-αFGL2 treatment does not cause toxicity in immunocompetent mice

To evaluate the suitability of FGL2 as a target for T cell therapy with low risk of off-tumor on-target toxicity, we assessed the expression of FGL2 in human GBM tissues and normal human tissue arrays using FGL2 mAb-clone #4 from which the αFGL2 construct was derived. As shown in Fig. 1e, FGL2 was highly expressed in human GBM tissues but not in healthy medulla oblongata tissues. In healthy tissue arrays (Fig. 1e), major organs such as the brain, lung, breast, spleen, and muscle were FGL2 negative, while moderate expression of FGL2 was observed in the stomach, colon, and pancreas. (Fig. 1e). To assess the potential toxicity of T-αFGL2, we intravenously injected 5 million T-Ctr or T-αFGL2 cells into non-tumor-bearing 7-week-old immunocompetent Balb/c mice. Five days after T cell injection, we evaluated blood chemistry, organ toxicities, and immune cell populations in the spleen and bone marrow. As shown in Supplementary Fig. 2a and b, mice treated with T-αFGL2 exhibited no significant changes in immune cell counts in either the spleen or bone marrow. T-αFGL2 treatment caused no abnormalities in blood chemistry (Supplementary Fig. 2c), but mice treated with T-Ctr had significantly higher blood levels of albumin ($P = 0.0264$) and globulin ($P = 0.0181$) than did untreated mice (Supplementary Fig. 2c). Furthermore, a board certified veterinary pathologist (N.W.F.) observed no evident abnomality or aberrant T lymphocyte infiltration in tissue sections following T-αFGL2 cell infusion (Supplementary Fig. 3 and Supplementary Table 1). Taken together, these results show that T-αFGL2 therapy does not cause detectable organ toxicity in immunocompetent mice.

T-αFGL2 therapy induces superior antitumor activity in vivo

To test the efficacy of T-αFGL2 therapy *in vivo*, we first validated expression of FGL2 in mouse GBM tissue. Brain tissues from immunocompetent syngeneic mouse GBM model (DBT tumor-bearing mice) were cryosectioned and stained with FGL2 mAb-clone #4. As shown in Fig. 2a, both tumor cells and surrounding stroma were positively stained for FGL2. Next, DBT-bearing Balb/c mice were used to evaluate the antitumor effects of T-αFGL2. Mice were inoculated with tumor cells and then treated with standard chemotherapy temozolomide (TMZ) on days 3, 4, and 5 to assimilate standard care, before administering T-Ctr or T-αFGL2 cells via the tail vein on days 6 and 13 after tumor cell inoculation (Fig. 2b). DBT is a very aggressive GBM tumor, and most DBT-bearing mice died within 3 weeks in the no treatment or T-Ctr group. T-αFGL2 treatment effectively suppressed DBT tumor progression, and tumors were eliminated in about 30% of the T-αFGL2–treated mice. These mice remained tumor free for up to 70 days before being used for a rechallenge study. In contrast, tumors progressed rapidly in T-Ctr–treated mice (Fig. 2c-e).

To confirm the anti-tumor efficacy of T-αFGL2 treatment, we also took advantage of another syngeneic mouse GL261 model. As shown in Fig. 2f-g, T-αFGL2 treatment, compared with T-Ctr treatment, suppressed this GBM tumor growth and extended mouse survival. Overall, T-αFGL2 showed superior antitumor properties in syngeneic malignant brain tumor models.

T-αFGL2 treatment induces formation of tumor-specific $CD8^+T_{RM}$ like cells in the brain

We next evaluated whether long-term survivors that had been treated with T-αFGL2 cells developed memory T cells that were reactive to tumor cells. We rechallenged T-αFGL2–treated survivors with an intracranial (i.c.) injection of DBT cells (Fig. 3a). The re-challenged DBT cells were cleared within 7 days in T-αFGL2–treated survivors (Fig. 3b), and local re-exposure to DBT cells induced a rapid, more than 18-fold increase in the number of $CD8^+$ T cells in the brains of T-αFGL2–treated survivors compared to the number in naïve brains (Fig. 3d, 3f). To investigate the tumor specificity of the generated memory T cells, we rechallenged DBT tumor-rejecting mice induced by T-αFGL2 treatment with 4T1 tumor cells (i.c.), which also developed tumors in the naïve balb/c mice rapidly. We found these DBT-rejecting memory T cells failed to protect mice from 4T1 tumor cell challenge (Supplementary Fig. 4a). This rapid and intense tumor reactivity to DBT cells, but not to 4T1 cells, confirmed that tumor-specific memory $CD8^+$ T cells had developed in the brains of T-αFGL2–treated survivors.

To determine whether these tumor-specific memory $CD8^+$ T cells stayed in the vicinity of the tumor (ie, in the brain) or migrated throughout the body, we inoculated DBT cells subcutaneously into the flanks of T-αFGL2 survivors and naïve mice (Fig. 3a). Interestingly, both groups of mice developed tumors under the skin (Fig. 3c), suggesting that the tumor-specific memory $CD8^+$ T cells in T-αFGL2–treated survivors were restricted to the brain. To confirm that tumor-reactive $CD8^+$ T cells only existed in the brain, we assessed T cells from the brains and draining lymph nodes (dLNs) of naïve mice and T-αFGL2–treated survivors 7 days after the rechallenge with DBT cells. As shown in Fig. 3d and e, the ratio of $CD8^+$ T cells to $CD4^+$ T

cells in the brain was up to 8-fold higher in T-αFGL2–treated survivors than in naïve mice. Moreover, the ratio of $CD8^+$ to $CD4^+$ T cells was 9-fold higher in the brains than in the LNs of T-αFGL2–treated survivors, suggesting that $CD8^+$ T cells, but not $CD4^+$ T cells, were the primary memory T cells controlling tumor cell growth, and that these $CD8^+$ T cells were only resident in the brain. Taken together, these data strongly indicate that T-αFGL2 treatment induced development of brain-resident tumor-specific $CD8^+T_{RM}$ like cells.

$CD8^+T_{RM}$ like cells undergo recall expansion and reject tumor cells when being transplanted into naïve brains

To validate that $CD8^+$ T cells in the brains of T-αFGL2–treated survivors were $CD8^+T_{RM}$ cells, we sorted $CD8^+$ T cells from the brains, draining lymph nodes (dLNs), and peripheral blood (PB) of T-αFGL2–treated survivors on day 7 after tumor cell inoculation and adoptively transplanted these T cells along with DBT cells directly into the brains (intracranially) of naïve recipient mice (Fig. 4a). In contrast to both dLN and PB $CD8^+$ T cells, which failed to mount a recall response, brain $CD8^+$ T cells underwent expansion even when reseeded in the brain tissue in low numbers (3000 cells) (Fig. 4b, c), confirming that the $CD8^+$ T cells in the brains of T-αFGL2–treated survivors are *bona fide* T_{RM} cells. As most of the $CD8^+$T cells in tumor experienced brains were $CD44^+$ memory T cells, while the $CD8^+$T cells in peripheral were not, we then compared the anti-tumor effect of $CD44^+CD8^+$T cells in brain, dLNs, pLNs and PB to validate the results. In consistence with $CD8^+$T cells, the $CD44^+CD8^+$T cells in peripheral tissues didn't show protection against tumor cells in vivo (Supplementary Fig. 4b and 4c). Similar results was found in GL261 model (Supplementary Fig. 4d). To determine whether $CD4^+$ T cells in the brain behaved in a similar manner as $CD8^+$ T cells, we sorted $CD4^+$ and $CD8^+$ T cells from the brains of T-αFGL2–treated survivors and then co-inoculated with DBT cells into the brains of naïve recipient mice. As shown in Fig. 4b and c, $CD4^+$ T cells did not have the same tumor-cell-eliminating capacity as $CD8^+$ T cells, confirming that the induced brain resident $CD8^+$ T cells, but not $CD4^+$ T cells, in the brain provide immune surveillance of the previously encountered antigen.

To further investigate whether the adoptively transplanted $CD8^+$ T_{RM} cells could survive and remain in the brains of naïve recipient mice, we subsequently challenged the recipient mice with tumor cells on day 40 after adoptive $CD8^+$ T cells transplantation. We observed that the recipient mice rejected the rechallenged tumor cells (Fig. 4d, e). These findings show that $CD8^+T_{RM}$ cells were successfully transplanted into naïve brains, transforming naïve brains to become tumor rejecting brains. To further validate the function of transplanted $CD8^+T_{RM}$ cells and exclude the effect of host T cells, we transplanted the lymphocytes from brain with T_{RM} (T_{RM}-BILs) into brain of naïve immunodeficient SCID mice and re-challenged these mice 35 days after the transplantation (Fig. 4f). The same as the parental T_{RM} bearing mice, these T_{RM} transplanted SCID mice showed anti-tumor capacity in the brain (Fig 4f-g); To verify the transplanted CD8+T cells are responsible for the protection, we re-challenged these SCID survivors with tumor cells combined with αCD8, αCD4 or αsialo GM1 antibodies to deplete $CD8^+$T cells, $CD4^+$T cells and NK cells

respectively. Only depleting $CD8^+$T cells, but not depleting $CD4^+$T cells or NK cells, impaired this protection (Fig 4h and 4i). Taken together, $CD8^+T_{RM}$ like cells, in brains of T-αFGL2–treated survivors, which fulfill both memory and reactive functions against tumor cells, are tumor specific brain $CD8^+T_{RM}$ cells. Notably, these $CD8^+$ T_{RM} cells can be adoptively transferred into the naïve brains with or without host T cells.

$CD8^+T_{RM}$ cells establish classical T_{RM} phenotype

To determine whether these $CD8^+T_{RM}$ like cells bear classical TRM phenotype, we checked CD69, CD103 and CD62L expression, which were used to identify T_{RM}[1,10,24]. To verify that the isolated BILs-$CD8^+$T cells were brain restricted, we performed i.v. injection of the CD8β antibody and found that over 90% of BILs-$CD8^+$T cells were non-circulating brain resident T cells (Supplementary Fig. 5a). Here, we found that compared with $CD44^+CD8^+$T cells in PB, the $CD44^+CD8^+$T cells in T_{RM} bearing brains with T_{RM} were $CD69^+$ (either $CD103^+$ or $CD103^-$), and $CD62L^-$(Fig. 4j). Similar results were found for $CD4^+$ T cells (Supplementary Fig. 5b). These findings show that $CD8^+T_{RM}$ like cells in brains established a classical T_{RM} phenotype of $CD69^+CD62L^-$. Together, both function and phenotype of the $CD8^+T_{RM}$ like cells in brains of T-αFGL2–treated survivors further validated that they are tumor specific brain $CD8^+T_{RM}$ cells.

The function of $CD8^+T_{RM}$ cells is TCR-MHC-I dependent

Since TCR is generated through random rearrangement of genomic V(D)J segments and is the mediator of antigen recognition and binding by T lymphocytes, we next questioned whether $CD8^+T_{RM}$ cells displayed a unique TCR repertoire that was distinct from that found in the dLNs. To this end, we sorted CD44+CD8+ T (memory CD8+T) cells from the brains and dLNs of T-αFGL2–treated survivors on day 20 after the third challenge with DBT cells via flow cytometric sorting, followed by TCRα and TCRβ deep sequencing (Fig. 5a). The most abundant T cell clones—those with a frequency of more than 5%—in T_{RM}-bearing brains constituted more than 60% of the total TCRα and TCRβ repertoire, whereas no T cell clones with a frequency of more than 5% were found in the TCRβ repertoire of $CD44^+CD8^+$ T cells in the dLNs (Supplementary Fig. 5c). To further characterize the TCR repertoires of T_{RM} cells and dLNs-$CD44^+CD8^+$ T cells, we analyzed sequences of complementarity determining region 3 (CDR3), which encompasses the V(D)J recombination junctions and encodes the vast majority of TCR variation. Moreover, all of the top 10 dominant CDR3 sequences in T_{RM} cells encompassed the V/J recombination, but each dominant CDR3 sequence in dLNs-$CD44^+CD8^+$ T cells encompassed a unique V/J recombination (Fig. 5b and Supplementary Fig. 5d). Analysis of the V and J domain usage showed that, in one of the T-αFGL2–treated survivors, the most dominant clone of TCRβ in T_{RM} cells was grouped by V17/J1-4, which was absent in dLNs (Fig. 5b). These data showed the presence and expansion of unique T cell clones and that there was no overlap of the highly occupied TCR clone in T_{RM} cells with the TCR clone in dLNs-$CD44^+CD8^+$ T cells. Interestingly, each mouse of T-αFGL2–treated survivors bears different T_{RM} clones

against different antigens. These data suggested that these highly expanded TCR repertoires of $CD8^+$ T_{RM} cells were associated, thus, with the rapid and robust response of T_{RM} cells against tumor cells.

To verify the robust response of $CD8^+T_{RM}$ cells against tumor cells is associated with the interaction between expanded TCR and MHC-I, we blocked MHC-I in vivo using αMHC-I antibody when transplanted $CD8^+T_{RM}$ cells into naïve mice. Blocking MHC-I abolished the anti-tumor efficacy of the transplanted $CD8^+T_{RM}$ cells (Fig 5c-f), demonstrating TCR-MHC-I interaction is required for the proper function of $CD8^+T_{RM}$ cells in vivo.

T-αFGL2 treatment-induced CD69 expression on $CD8^+$ memory T cells is essential for $CD8^+T_{RM}$ formation

To understand the cellular mechanisms by which the FGL2-blocking scFv induces the generation of $CD8^+T_{RM}$ cells, on day 4 after the second T cell infusion, we performed high-dimensional profiling of brain-infiltrating lymphocytes (BILs) using time-of-flight mass cytometry (CyTOF) with a panel of 37 antibodies that illustrated different immune populations (Fig. 6a). CyTOF data analysis divided BILs into 15 immune cell populations (Fig. 6b). As $CD8^+$ T cells are the primary functional cells rejecting tumor cells as shown in our transplant study (Fig. 4b), we focused on these cell populations. We found that the $CD8^+$ T cell population was composed of 2 subpopulations: $CD69^+CD8^+$ memory T cells ($CD69^+CD8^+$ T_M) and $CD69^-CD8^+$ memory T cells ($CD69^-CD8^+$ T_M) (Fig. 6b). Notably, the subset of $CD69^+CD8^+$ T_M cells was significantly larger in mice that underwent T-αFGL2 treatment than in those that received T-Ctr treatment (Fig. 6c, d). Indeed, CD69 has been reported to help in the retention of memory T cells in resident tissues through inhibiting expression of the S1P receptor, which can promote T cell circulation into the blood; high level expression of CD69 on T cells is an indicator of T_{RM} cells[24]. To further determine the phenotype of these $CD69^+CD8^+$ T_M cells, we compared their expression of T cell exhaustion markers with that of $CD69^-CD8^+$ T_M cells. As shown in Fig. 6e, $CD69^+CD8^+$ T_M cells had higher levels of Ki67, CD223 (LAG3), and CD279 (PD-1) than did $CD69^-CD8^+$ T_M cells. This $CD69^{Hi}PD\text{-}1^{Hi}LAG3^{Hi}$ phenotype of highly proliferating $CD69^+CD8^+$ T_M cells has been reported to be most prominent in cells with T_{RM} characteristics in different kinds of tissues, including lung[15,25,26], breast[19], and skin[6]. These data indicated that T-αFGL2 treatment increased proliferating $CD69^+CD8^+$ T_M subsets with T_{RM} characteristics, which may promote the transformation of these $CD69^+CD8^+$ T_M cells into T_{RM} cells in the brain. To further validate the biological function of CD69 on $CD8^+T_{RM}$, we blocked CD69 in vivo by αCD69 antibody. When transplanted the $CD69^+CD8^+T_{RM}$ cells with tumor cells into naïve mice i.c., we found αCD69 antibody treatment didn't disrupt the anti-tumor efficacy of $CD8^+T_{RM}$ cells. However, when we re-challenge these mice with tumor cells i.c. on day 60 post the transplantation, the mice treated with αCD69 antibody lost the tumor-rejecting capacity (Fig. 6f-g), indicating that CD69 doesn't affect the executive function of T_{RM} but is required for the prolonged residence and function of $CD8^+T_{RM}$ in brains.

Besides $CD8^+$ T cells, we analyzed the other immune subpopulations, including helper T cells (Th cells) and regulatory T cells (Tregs), DCs, macrophages, monocytes, and neutrophils. However, no significant difference in these subpopulations was observed between the T-αFGL2 and T-Ctr groups (Supplementary Fig. 6), suggesting that the antitumor effect induced by T-αFGL2 treatment is different from antibody therapy and may work mainly through regulating $CD69^+CD8^+$ T_M cells.

T-αFGL2 induced $CD8^+T_{RM}$ formation is associated with CXCL9/10-CXCR3 axis

To further understand the molecular mechanism by which FGL2-blocking scFv induces $CD69^+CD8^+T_M$ cells generation, we analyzed the CYTOF data for the chemokine receptors (i.e. CCR2, CXCR3, CXCR2, and CX3CR1) that may affect the T cells infiltration and recruitment to tumor sites. Intriguingly, we found that T-αFGL2 treatment increased CXCR3 expression on $CD69^+CD8^+T_M$ cells in tumor bearing brains, compared with T-Ctr treatment (Fig. 7a). Flow cytometry data also verified that T-αFGL2 treatment, compared with T-Ctr, increased proportion of $CXCR3^+CD69^+CD8^+$T cells among total $CD8^+$T cells in tumor bearing brains (Fig. 7b), indicating that increased CXCR3 expression on CD8T cells may play a role in mediating T-αFGL2 induced $CD69^+CD8^+T_{RM}$ cells formation. To validate this notion, we compared the anti-tumor efficacy of T-αFGL2 in treating tumor bearing wild type (WT) mice and CXCR3 deficient ($CXCR3^{-/-}$) mice. T-αFGL2 treatment didn't show protective effect in $CXCR3^{-/-}$ mice as did in WT mice (Fig. 7c). Besides, the $CD69^+CD8^+T_M$ population was reduced in $CXCR3^{-/-}$ mice compared with WT mice (Fig. 7d), suggesting that CXCR3 play a critical role in mediating T-αFGL2 induced $CD69^+CD8^+T_M$ cells generation and thus $CD8^+T_{RM}$ formation for protective function.

To characterize how the CXCR3 chemokine system mediates anti-tumor responses to T-αFGL2 treatment, we examined the expression of the CXCR3 chemokine ligands CXCL9 and CXCL10. Protein levels of CXCL9 and CXCL10 were markedly increased in tumor bearing brains after T-αFGL2 treatment compared to T-Ctr treatment (Fig. 7e). To determine the roles of CXCL9 and CXCL10 in T-αFGL2 induced tumor rejection and $CD8^+T_{RM}$ formation, we used αCXCL9 and αCXCL10 antibodies to blocking CXCL9 and CXCL10 in vivo. Consistent with our earlier findings (Fig. 7c-d), the therapeutic benefits of T-αFGL2 was lost when blocking CXCL9 and CXCL10 (Fig. 7f), indicating a critical role for CXCL9 and CXCL10 in T-αFGL2 immunotherapy. Moreover, the percentage of $CD69^+CD8^+T_M$ was increased upon T-αFGL2 treatment in control IgG group but not in αCXCL9 and αCXCL10 antibodies treatment group (Fig .7g), indicating the functional importance of CXCL9/10-CXCR3 axis for response to T-αFGL2 therapy and $CD8^+T_{RM}$ formation. Altogether, T-αFGL2 therapy induced tumor-reactive T cells' proliferation, secretion of granzyme B to control tumor progression, and increased CXCR3, CD69 expression on memory CD8+T cells to help them retain in the brains, which will foster the formation of tumor specific brain resident $CD8^+$TRM (Fig. 7h).

Discussion

Increasing evidence has shown that T_{RM} cells have a promising role in the control of solid tumors[27]. Early studies showed that intravaginal vaccination induced T_{RM} formation in cervicovaginal tissues resulting in the control of tumors in the genital tract[28]. Nonetheless, whether adoptive cellular therapies (ACT) can foster T cells' development into T_{RM} cells remains unknown. Our study has provided an ACT-based treatment, T-αFGL2 cell therapy, which can program endogenous T cells into tumor specific $CD8^+T_{RM}$ cells. These T_{RM} cells had a highly expanded and specific TCR repertoire. After being transplanted into the brains of either immunocompetent or T cell deficient naïve mice, these T_{RM} cells transformed naïve mice to become tumor rejecting in the brains but not in peripheral tissues due to the tissue specific resident nature.

Retention in the resident tissue is required for T_{RM} cells to expand and to be functional[10]. One of the mechanisms of T_{RM} retention is adhesion to home tissue, which is associated with overexpression of integrin molecules such as LFA-1 (αLβ2)[18], VLA-1(α1β1)[29], and CD103 (αEβ7)[10,29], binding to adhesion molecules on the endothelium, and the extracellular matrix components collagen and laminin. Another mechanism attributed to retention of T_{RM} in the tissue is unresponsiveness to signals that promote recirculation. Expression of S1PR1 (encoded by *S1pr1*)[30], CD62L (encoded by *Sell*)[31], and CCR7 (encoded by *Ccr7*)[32] permits recirculation of memory T cells. It has been reported that CD69 suppresses memory T cells' recirculation potential by inhibiting surface expression of the S1P receptor[24]. Indeed, most T_{RM} cells constitutively express CD69[5,9,33]. Although CD103, which binds to E-cadherin on epithelial cells, is expressed on the most-studied T_{RM} cells reside in epithelial tissue[29], CD69 is more commonly used than CD103 to identify T_{RM} cells in non-lymph organs. In our study, T-αFGL2, compared with T-Ctr, increased the population of $CD69^+CD8^+$ T_{RM} like cells ($Ki67^{Hi}PD\text{-}1^{Hi}LAG3^{Hi}$) in the brain tumor environment (Fig. 6b-d). The T-αFGL2 treatment induced $CD8^+T_{RM}$ (phenotype: $CD69^+CD62L^-$). Blocking CD69 appears to disrupt the residence of the brain-resident T_{RM} cells (Fig. 6f-g). Altogether, the increased tissue retention molecule CD69 expression on $CD8^+$ T_M cells in the brain can help retain these cells in the brain and promote their differentiation into brain-resident T_{RM} cells.

T-aFGL2 treatment-induced $CD69^+CD8^+T_{RM}$ formation is associated with CXCL9/10-CXCR3 axis, as either absence of CXCR3 or blocking CXCL9/10 abrogated the increased $CD69^+CD8^+T_M$ after T-aFGL2 treatment, and thus interrupted the anti-tumor efficacy of T-aFGL2 treatment (Fig. 7). The notion that CXCR3-CXCL9/10 axis promotes the generation of T_{RM} is consistent with the previous findings that CXCR3-CXCL9 axis is required for reinvigoration of intratumoral $CD8^+$ T cell responses in response to PD-1 blockade[34], and exogenous application of CXCR3 ligands promoted the T_{RM} cells formation in the epithelium of the lower female reproductive tract[35].

It's reported that the immune suppressive FGL2 limits cytotoxic $CD8^+$ T-cell responses via FcγRIIb[36]. To evaluate if the T cells express FcγRIIb, which can bind and be regulated by FGL2 in tumor microenvironment in our study, we detected the FcγRIIB expression on T cells in DBT tumor bearing

brains. T cells, both $CD4^+$T cells and $CD8^+$T cells, express FcγRIIB, though not all of them (Supplementary Fig. 7a). Moreover, wt T cells, but not FcγRIIB $^{-/-}$ T cells, can directly bind the FGL2 that is anchored on the chip via biotin-streptavidin interaction (supplementary Fig. 7b), verifying that T cells can directly bind FGL2 through FcγRIIB. Besides, T-aFGL2 treatment lost the superior anti-tumor effect, compared with T-Ctr, in FcγRIIB $^{-/-}$ mice (supplementary Fig. 7c), suggesting that FcγRIIB was regulated by FGL2. These data suggested that T cells in this study can bind and be regulated by FGL2 in tumor microenvironment through FcγRIIB, and T-aFGL2 treatment can disrupt this FcγRIIB-FGL2 interaction and boost the cytotoxic T cells responses.

To date, most studies of T_{RM} cells have focused on autoimmune diseases and infections. For example Malik *et al.* reported that melanoma antigen-specific skin-resident memory T cells are maintained in vitiligo-afflicted skin[37], but no adoptive cellular therapy that induces tumor-specific T_{RM} cells has yet been evaluated. Here, we performed T-αFGL2 adoptive cell treatment to brain tumor-bearing mice, and found that T-αFGL2 induced tumor-specific $CD8^+T_{RM}$ cells in the brain. The phenotype of these $CD8^+T_{RM}$ cells were either $CD69^+CD103^+$ or $CD69^+CD103^-$. Besides the phenotype of these tumor-specific T_{RM} cells, we also characterized their TCR repertoire. TCR recognizes antigens presented by the major histocompatibility complex (MHC) on antigen-presenting cells and subsequently activates T cells and mediates the eradication of the antigen[38–41]. However, the TCR repertoires of tumor-specific T_{RM} cells have not previously been characterized. From next generation RNA sequencing, we noted that the $CD8^+T_{RM}$ cells had a highly expanded TCRαβ repertoire (Fig. 5). Moreover, no overlap of the TCR clone was found between T_{RM} cells in the brain and memory T cells in the periphery. This is distinct from influenza-specific lung-resident memory T cells, which maintain a wide diversity of TCR profiles[13]. Blocking MHC-I abolished the anti-tumor efficacy of the CD8 + T_{RM} cells (Fig. 5c-f), demonstrating TCR-MHC-I interaction is required for the proper function of $CD8^+T_{RM}$ cells in vivo. Further functional evaluation of this highly expanded TCR repertoire on T_{RM} cells will be an important part of future studies.

T_{RM} cells occupy frontline sites of infection and are positioned to respond most immediately and potently. The abundance of cells with T_{RM} cell characteristics in tumors often correlates with a favorable outcome[19,42–44]; thus, promoting tumor-specific T_{RM} cell formation in tumor tissues or adoptively transferring tumor-specific T_{RM} cells into tumor sites are promising approaches for treating patients with cancer. Wakim *et al.* found that virus-specific T_{RM} cells in the brain die rapidly upon isolation from the resident tissue and fail to undergo recall expansion after adoptive transfer into the bloodstream of an antigen-challenged recipient, indicating that these cells depend on the local milieu for their function and survival[12,45]. Here, we were able to transfer $CD8^+T_{RM}$ cells into the brains of both immuocompetent and T cells deficient naïve mice and induce a tumor-specific reaction in the recipient mice (Fig. 4). To our knowledge, this is the first study in which tumor-specific $CD8^+T_{RM}$ cells were successfully transferred into the same tissue of naïve mice *in vivo*. Our success may be explained by the following factors: (1) T_{RM} cells should be transferred into the same tissue in naïve mice where the T_{RM} cells originally resided; (2)

T_{RM} cells should be cotransferred with antigens that can activate them. Besides yielding novel insights into these tumor specific brain resident $CD8^{+}T_{RM}$ cells, our study provides a valuable resource for further investigations of tumor-specific T_{RM} cell formation in the brain. Such studies will ultimately aid the development of strategies for immunotherapy of brain cancers.

Declarations

Acknowledgments

We appreciate Scientific Publications, Research Medical Library at MD Anderson for helping us edit our manuscript. We thank Dr. Leonid Metelitsa (Baylor College of Medicine) for providing DBT mouse glioma cells. for This research used the Flow Cytometry, Cellular Imaging Facility and DNA analysis Core Facility, Monoclonal Antibody Core Facility at MD Anderson, which are supported in part by the National Institutes of Health through MD Anderson's Cancer Center Support Grant P30 CA016672. Core Grant Citation. This work was supported by National Institutes of Health Grants R01 CA120895 and R01 CA200574.

Authors' contributions

QZ and SL conceived and designed the experiments. QZ, LK, NWF, JY, JH, ZJ and XX conducted the experiments. RH were responsible for the mouse model. QZ, SJ, XT, and JW analyzed the data. QZ, SL, ABH, SY, LD, DM and HO edited and/or drafted the manuscript. SL supervised the study. All authors have read and approved the final version of the manuscript.

References

1. Amsen, D., van Gisbergen, K., Hombrink, P. & van Lier, R. A. W. Tissue-resident memory T cells at the center of immunity to solid tumors. Nat Immunol **19**, 538–546, doi:10.1038/s41590-018-0114-2 (2018).
2. Masopust, D., Vezys, V., Marzo, A. L. & Lefrançois, L. Preferential localization of effector memory cells in nonlymphoid tissue. Science **291**, 2413–2417 (2001).
3. Watanabe, R. *et al.* Human skin is protected by four functionally and phenotypically discrete populations of resident and recirculating memory T cells. *Science translational medicine* **7**, 279ra239-279ra239 (2015).
4. Welten, S. P. M., Sandu, I., Baumann, N. S. & Oxenius, A. Memory CD8 T cell inflation vs tissue-resident memory T cells: Same patrollers, same controllers? Immunol Rev **283**, 161–175, doi:10.1111/imr.12649 (2018).
5. Beura, L. K. *et al.* CD4(+) resident memory T cells dominate immunosurveillance and orchestrate local recall responses. J Exp Med **216**, 1214–1229, doi:10.1084/jem.20181365 (2019).
6. Dijkgraaf, F. E. *et al.* Tissue patrol by resident memory CD8(+) T cells in human skin. Nat Immunol **20**, 756–764, doi:10.1038/s41590-019-0404-3 (2019).

7. Menares, E. *et al.* Tissue-resident memory CD8(+) T cells amplify anti-tumor immunity by triggering antigen spreading through dendritic cells. Nat Commun **10**, 4401, doi:10.1038/s41467-019-12319-x (2019).
8. Park, S. L. *et al.* Tissue-resident memory CD8(+) T cells promote melanoma-immune equilibrium in skin. Nature **565**, 366–371, doi:10.1038/s41586-018-0812-9 (2019).
9. Schenkel, J. M. & Masopust, D. Tissue-resident memory T cells. Immunity **41**, 886–897, doi:10.1016/j.immuni.2014.12.007 (2014).
10. Mackay, L. K. *et al.* The developmental pathway for CD103(+)CD8 + tissue-resident memory T cells of skin. Nat Immunol **14**, 1294–1301, doi:10.1038/ni.2744 (2013).
11. Gaide, O. *et al.* Common clonal origin of central and resident memory T cells following skin immunization. Nat Med **21**, 647–653, doi:10.1038/nm.3860 (2015).
12. Wakim, L. M. *et al.* The molecular signature of tissue resident memory CD8 T cells isolated from the brain. J Immunol **189**, 3462–3471, doi:10.4049/jimmunol.1201305 (2012).
13. Pizzolla, A. *et al.* Influenza-specific lung-resident memory T cells are proliferative and polyfunctional and maintain diverse TCR profiles. J Clin Invest **128**, 721–733, doi:10.1172/JCI96957 (2018).
14. Zens, K. D., Chen, J. K. & Farber, D. L. Vaccine-generated lung tissue–resident memory T cells provide heterosubtypic protection to influenza infection. *JCI insight* **1** (2016).
15. Clarke, J. *et al.* Single-cell transcriptomic analysis of tissue-resident memory T cells in human lung cancer. J Exp Med **216**, 2128–2149, doi:10.1084/jem.20190249 (2019).
16. Vieira Braga, F. A. *et al.* A cellular census of human lungs identifies novel cell states in health and in asthma. Nat Med **25**, 1153–1163, doi:10.1038/s41591-019-0468-5 (2019).
17. Hayward, S. L. *et al.* Environmental cues regulate epigenetic reprogramming of airway-resident memory CD8 + T cells. Nature Immunology, 1–12 (2020).
18. McNamara, H. *et al.* Up-regulation of LFA-1 allows liver-resident memory T cells to patrol and remain in the hepatic sinusoids. Science Immunology **2** (2017).
19. Savas, P. *et al.* Single-cell profiling of breast cancer T cells reveals a tissue-resident memory subset associated with improved prognosis. Nat Med **24**, 986–993, doi:10.1038/s41591-018-0078-7 (2018).
20. Hu, J. *et al.* The duality of Fgl2-secreted immune checkpoint regulator versus membrane-associated procoagulant: therapeutic potential and implications. International reviews of immunology **35**, 325–339 (2016).
21. Latha, K. *et al.* The role of fibrinogen-like protein 2 on immunosuppression and malignant progression in glioma. JNCI: Journal of the National Cancer Institute **111**, 292–300 (2019).
22. Yan, J. *et al.* FGL2 as a multimodality regulator of tumor-mediated immune suppression and therapeutic target in gliomas. Journal of the National Cancer Institute **107**, djv137 (2015).
23. Yan, J. *et al.* FGL2 promotes tumor progression in the CNS by suppressing CD103 + dendritic cell differentiation. Nature communications **10**, 1–15 (2019).

24. Mackay, L. K. *et al.* Cutting edge: CD69 interference with sphingosine-1-phosphate receptor function regulates peripheral T cell retention. The Journal of Immunology **194**, 2059–2063 (2015).
25. Hombrink, P. *et al.* Programs for the persistence, vigilance and control of human CD8 + lung-resident memory T cells. Nature immunology **17**, 1467 (2016).
26. Wang, Z. *et al.* PD-1hi CD8 + resident memory T cells balance immunity and fibrotic sequelae. Science immunology **4**, eaaw1217 (2019).
27. Amsen, D., van Gisbergen, K. P., Hombrink, P. & van Lier, R. A. Tissue-resident memory T cells at the center of immunity to solid tumors. Nature immunology **19**, 538–546 (2018).
28. Sun, Y.-Y. *et al.* Local HPV recombinant vaccinia boost following priming with an HPV DNA vaccine enhances local HPV-specific CD8 + T-cell–mediated tumor control in the genital tract. Clinical Cancer Research **22**, 657–669 (2016).
29. Gebhardt, T. *et al.* Memory T cells in nonlymphoid tissue that provide enhanced local immunity during infection with herpes simplex virus. Nature immunology **10**, 524 (2009).
30. Skon, C. N. *et al.* Transcriptional downregulation of S1pr1 is required for the establishment of resident memory CD8 + T cells. Nat Immunol **14**, 1285–1293, doi:10.1038/ni.2745 (2013).
31. Gebhardt, T. *et al.* Different patterns of peripheral migration by memory CD4 + and CD8 + T cells. Nature **477**, 216–219 (2011).
32. Kumar, B. V. *et al.* Human tissue-resident memory T cells are defined by core transcriptional and functional signatures in lymphoid and mucosal sites. Cell reports **20**, 2921–2934 (2017).
33. Buggert, M. *et al.* Identification and characterization of HIV-specific resident memory CD8 + T cells in human lymphoid tissue. Science immunology **3**, eaar4526 (2018).
34. Chow, M. T. *et al.* Intratumoral activity of the CXCR3 chemokine system is required for the efficacy of anti-PD-1 therapy. Immunity **50**, 1498–1512. e1495 (2019).
35. Shin, H. & Iwasaki, A. A vaccine strategy that protects against genital herpes by establishing local memory T cells. Nature **491**, 463–467 (2012).
36. Morris, A. B. *et al.* Signaling through the inhibitory Fc receptor FcγRIIB induces CD8 + T cell apoptosis to limit T cell immunity. *Immunity* **52**, 136–150. e136 (2020).
37. Malik, B. T. *et al.* Resident memory T cells in the skin mediate durable immunity to melanoma. Sci Immunol **2**, doi:10.1126/sciimmunol.aam6346 (2017).
38. Zhang, L. *et al.* Lineage tracking reveals dynamic relationships of T cells in colorectal cancer. Nature **564**, 268–272, doi:10.1038/s41586-018-0694-x (2018).
39. Ahmadzadeh, M. *et al.* Tumor-infiltrating human CD4 + regulatory T cells display a distinct TCR repertoire and exhibit tumor and neoantigen reactivity. Science immunology **4** (2019).
40. Scheper, W. *et al.* Low and variable tumor reactivity of the intratumoral TCR repertoire in human cancers. Nature medicine **25**, 89–94 (2019).
41. Reuben, A. *et al.* Comprehensive T cell repertoire characterization of non-small cell lung cancer. Nature Communications **11**, 1–13 (2020).

42. Djenidi, F. *et al.* CD8 + CD103 + tumor–infiltrating lymphocytes are tumor-specific tissue-resident memory T cells and a prognostic factor for survival in lung cancer patients. The Journal of Immunology **194**, 3475–3486 (2015).
43. Webb, J. R., Milne, K., Watson, P., DeLeeuw, R. J. & Nelson, B. H. Tumor-infiltrating lymphocytes expressing the tissue resident memory marker CD103 are associated with increased survival in high-grade serous ovarian cancer. Clinical cancer research **20**, 434–444 (2014).
44. Nizard, M. *et al.* Induction of resident memory T cells enhances the efficacy of cancer vaccine. Nature communications **8**, 1–11 (2017).
45. Wakim, L. M., Woodward-Davis, A. & Bevan, M. J. Memory T cells persisting within the brain after local infection show functional adaptations to their tissue of residence. Proc Natl Acad Sci U S A **107**, 17872–17879, doi:10.1073/pnas.1010201107 (2010).

Figures

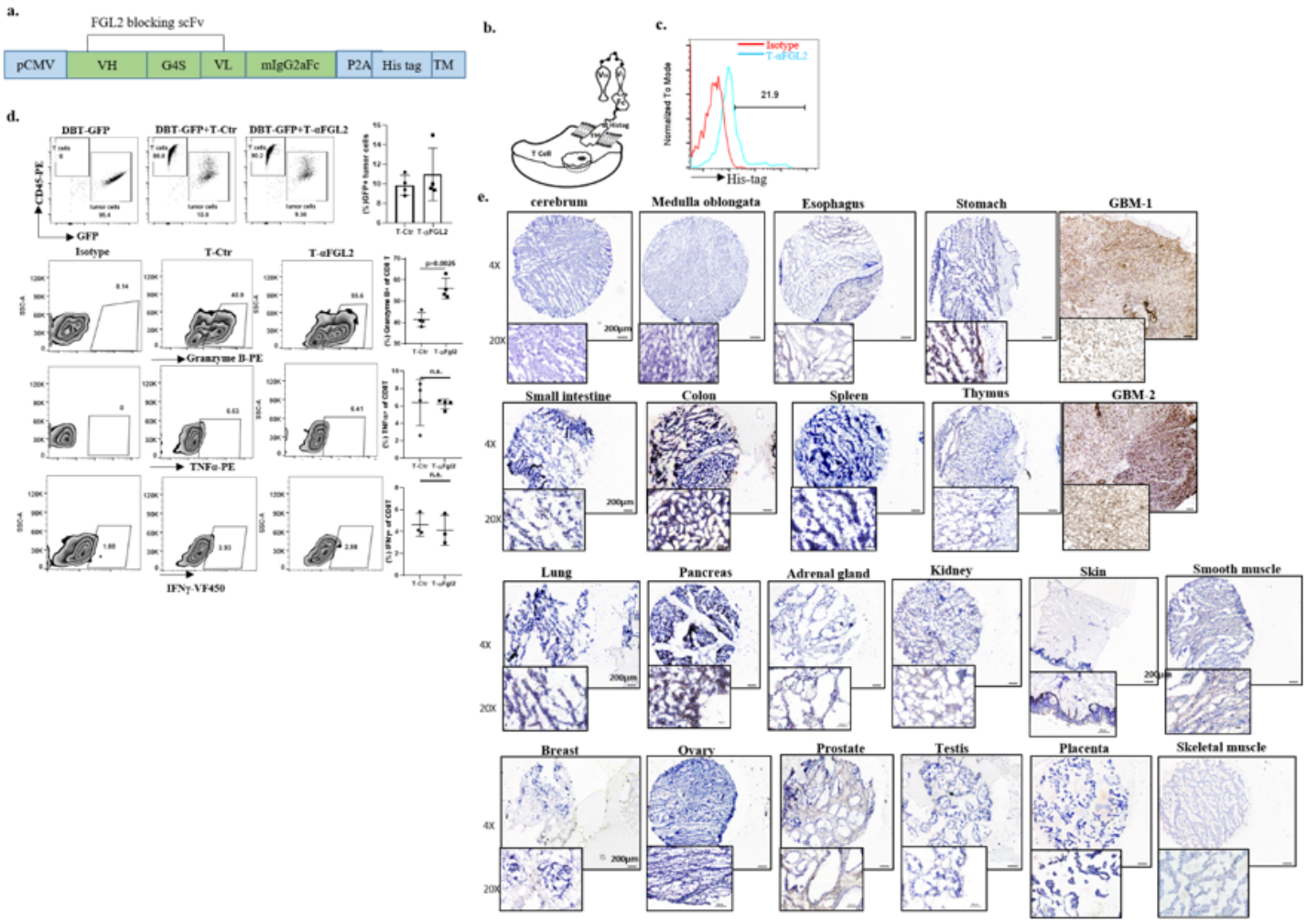

Figure 1

Specific functional antitumor activity of T-αFGL2 *in vitro*.

a, Schematic of the vector encoding the FGL2-blocking scFv, linked to the transmembrane (TM) domain. The His-tag domain was used for detection of the scFv. The Ctr vector is the empty CMV constract. G4S: pentapeptide GGGGS; P2A: porcine teschovirus-1. **b**, Cartoon schematic of a T cell transfected with the FGL2-blocking scFv vector (T-αFgl2). **c**, Representative flow cytometry histograms demonstrating FGL2-blocking scFv expression on mouse T cells following transduction. The scFv was detected with His-tag specific antibodies. **d**, Flow cytometry plots depicting no difference in proportion of tumor cells (DBT-GFP+) cocultured with T-Ctr and T-αFGL2 cells at E:T ratio of 4:1 for 72hrs (top panel); flow cytometry plots depicting increased granzyme B expression in T-αFGL2 cells (compared with T-Ctr) cocultured with DBT tumor cells at a ratio of 1:1 for 24 h; no difference in TNFα or IFNγ was detected between T-αFGL2 and T-Ctr. Data shown are mean ± SEM from 3 independent experiments. $^{**}P = 0.0025$, two-way t-test. NS, not significant. **e,** Representative micrographs of FGL2 expression in GBM and the indicated normal human tissues assessed by staining with FGL2 mAb-clone #4 at the final concentration of 1 μg/mL. Micrographs are representative of at least two sections per tissue. Scale bars, 100 μm.

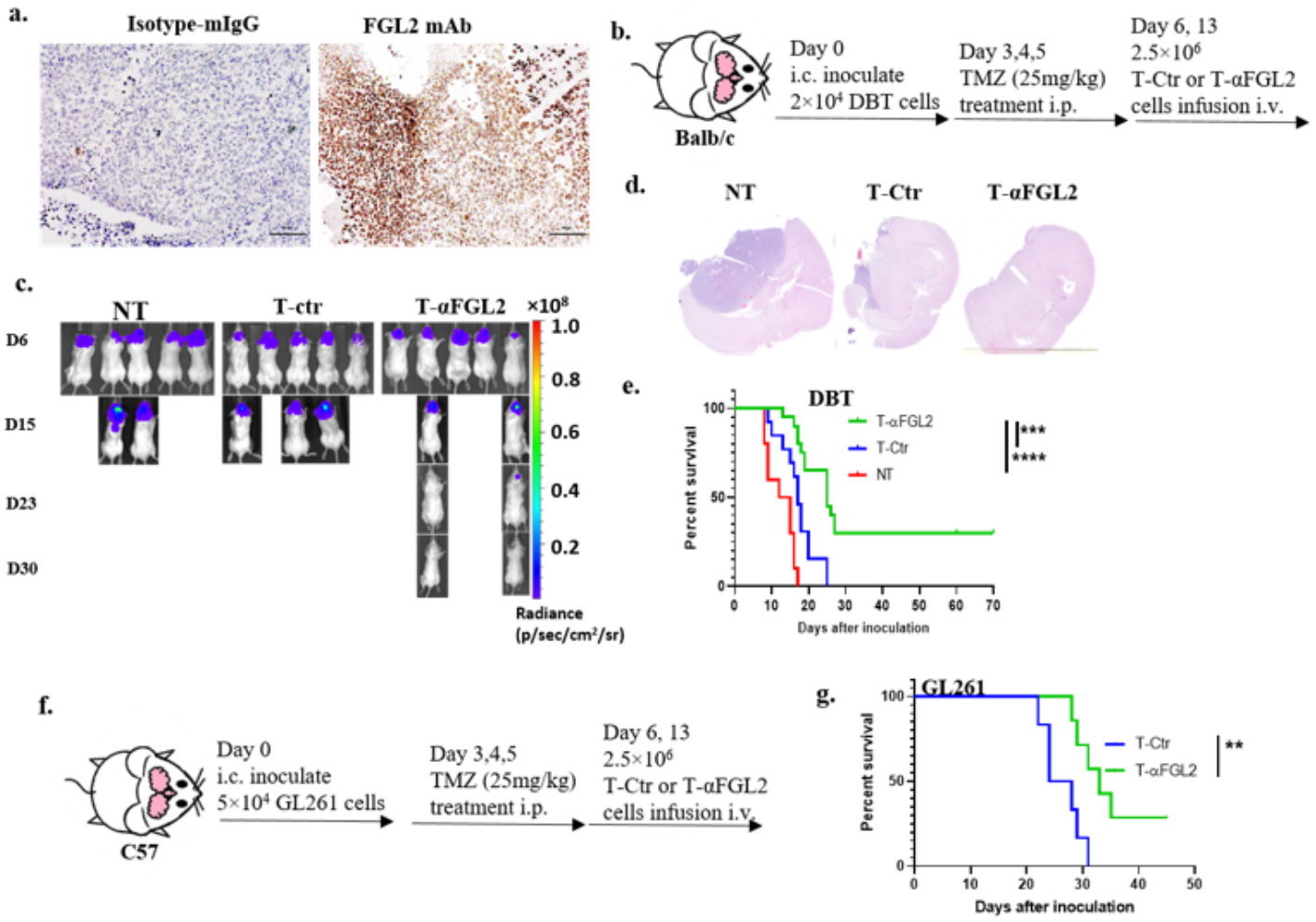

Figure 2

Antitumor activity of T-αFGL2 *in vivo*.

a, Representative micrographs of FGL2 expression in mouse brains with glioma assessed by staining with FGL2 mAb-clone #4 at the final concentration of 1 μg/mL. Slides stained without a primary Ab were used as negative controls. Scale bars, 50 μm. **b**, Schematic of the orthotopic glioma DBT model treated with temozolomide (TMZ) on days 3, 4, and 5 after tumor cell inoculation, followed by infusion of T-Ctr or T-αFGL2 on days 6 and 13. **c**, Representative bioluminescence images of DBT-luc tumor growth in the orthotopic glioma model shown in **b**. **d**, Representative H&E staining of brains from the orthotopic glioma model shown in **b** collected on day 14 after tumor cell inoculation. **e**, Kaplan-Meier survival curves of mice shown in **b** (n = 11-15 mice/group). ***P = 0.0002 (T-αFGL2 vs T-Ctr), ****P < 0.0001 (T-αFGL2 vs no treatment [NT] group), log-rank test. **f**, Schematic of the orthotopic glioma GL261 model. **g**, Kaplan-Meier survival curves of mice in **f** (n = 6~7 mice/group). **P = 0.0099 log-rank test.

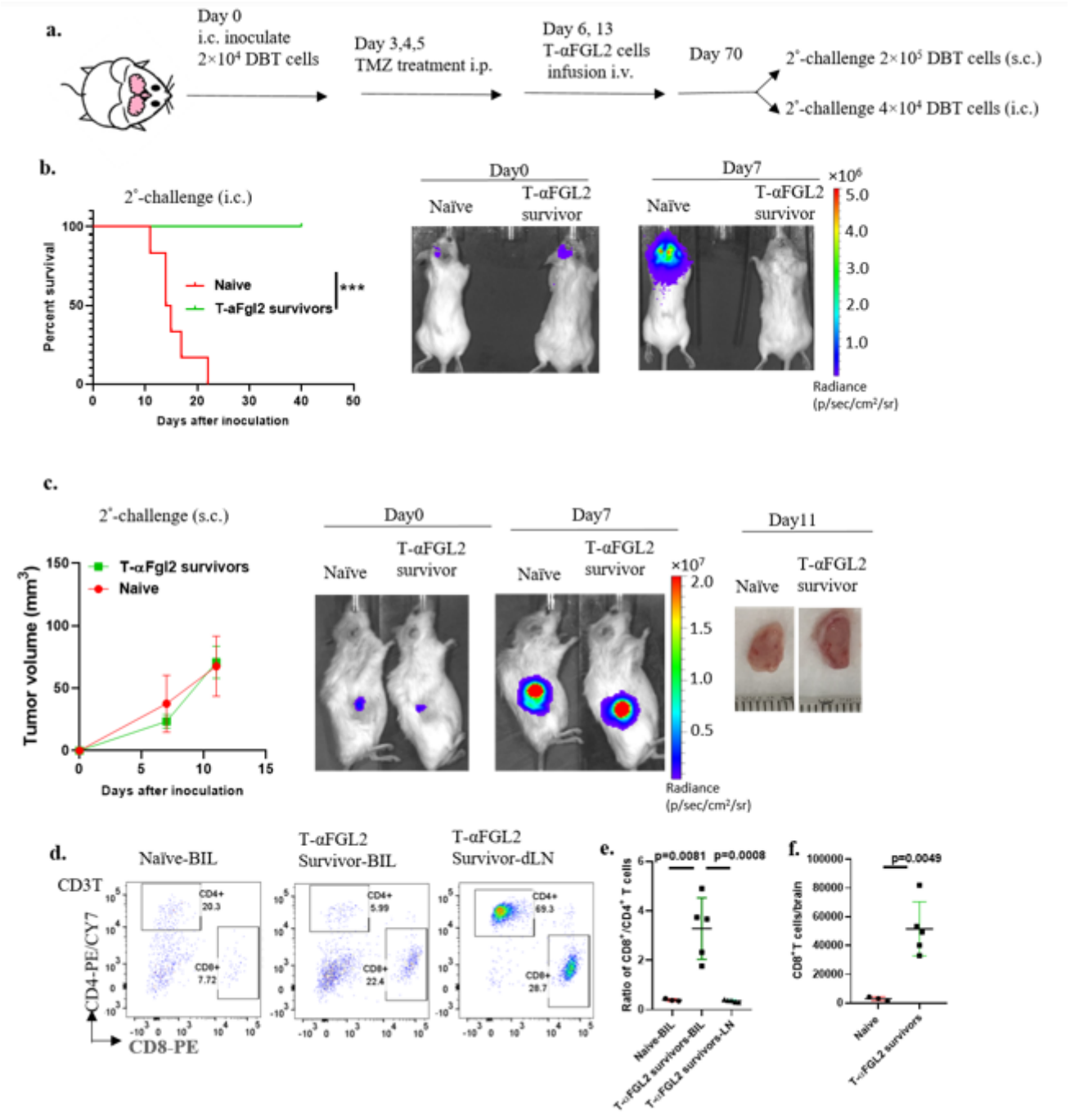

Figure 3

T-αFGL2 treatment induced brain-resident tumor-specific memory T cells.

a, Schematic of re-challenge with tumor cells, either subcutaneously (s.c.) or intracranially (i.c.), in the long-term survivors of the orthotopic glioma DBT model on day 70 after first tumor cell inoculation. **b**, Kaplan-Meier survival curves (left) and representative bioluminescence images (right) of mice shown in **a** on day 0 and day 7 after second tumor cell inoculation (i.c.) (n = 6). ***P = 0.0005, log-rank test. **c**, Tumor volume (left), representative bioluminescence images (middle) of mice on day 0 and day 7 after second tumor cell inoculation, and representative tumors (right) collected on day 11 after second tumor cell inoculation (s.c.) from the flanks of Balb/c mice. **d**, Representative flow cytometry plots depicting increase of $CD8^+$ T cells in the brains (BIL) of long-term survivors treated with T-αFGL2 (T-αFGL2 survivor). LN, lymph node. **e**, Graph showing the ratio of $CD8^+$ T cells to $CD4^+$ T cells in the brains of naïve mice and T-αFGL2 survivors and the LNs of T-αFGL2 survivors (n = 3-5 mice/group), two-way t-test. **f**, Graph showing $CD8^+$ T cell numbers in the brains of naïve mice and T-αFGL2 survivors (n = 3-5 mice/group), two-way t-test.

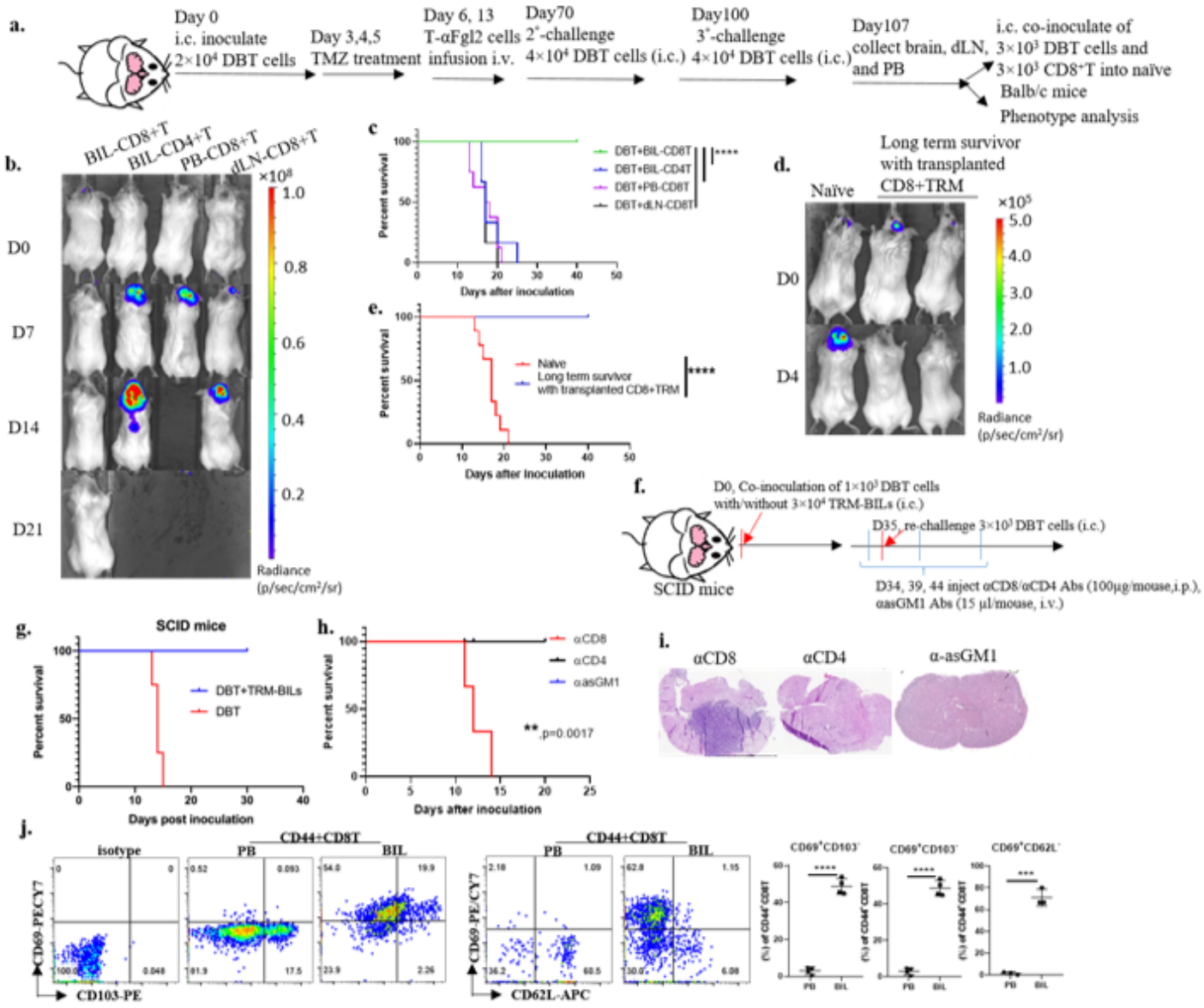

Figure 4

T_{RM}-like cells can be adoptively transferred.

a, Schematic of experimental design. T-αFGL2–treated survivors were rechallenged with DBT tumor cells intracranially (i.c.) on days 70 and 100 after the first tumor cell inoculation. On day 7 after the third challenge with tumor cells, the mice were euthanized, and their brains, draining lymph nodes (dLN), and peripheral blood (PB) were collected. **b**, Representative bioluminescence images of naïve Balb/c mice coinoculated i.c. with 3 × 10^3 DBT glioma cells and 3 × 10^3 T cells. Images show gliomas in mice coinoculated with $CD8^+$ T cells in the brain (BIL-$CD8^+$T), $CD4^+$ T cells in the brain (BIL-$CD4^+$T), $CD8^+$ T cells in peripheral blood (PB-$CD8^+$T), and $CD8^+$ T cells in draining lymph nodes (dLN-$CD8^+$T). $CD8^+$ T cells and $CD4^+$ T cells were sorted by flow cytometry on day 7 after the third challenge in T-αFGL2 survivors. **c**, Kaplan-Meier survival curves for mice in **b** (n = 8-9 mice/group). ****P < 0.0001, log-rank test. **d**, Representative bioluminescence images of naïve Balb/c mice and mice bearing transplanted BIL-$CD8^+$T

cells on days 0 and 4 after i.c. re-challenge with DBT cells on day 30 after BIL-$CD8^+$T cells transplantation. **e**, Kaplan-Meier survival curves of mice in **d** (*n* = 9 mice/group). ****$P < 0.0001$, log-rank test. **f**, Schematic of experimental design. 3×10^4 T_{RM} containing brain infiltrated lymphocyte cells (T_{RM}-BIL) were sorted by flow cytometry on day 7 after the third challenge in T-αFGL2 survivors, and coinoculated i.c. with 3×10^3 DBT cells into the naïve SCID mice; 35 days after the transplantation, the SCID mice with transplanted T_{RM}-BILs were re-challenged with 3×10^3 DBT cells i.c. combined with antibodies blocking CD8, CD4 or asGM1 i.p. **g**, Kaplan-Meier survival curves of mice in **f** (*n* = 4~6 mice/group). ***$P = 0.0003$, log-rank test. **h**, Kaplan-Meier survival curves of of SCID mice bearing transplanted T_{RM}-BILs cells i.c. re-challenged with DBT cells combined with antibodies blocking CD8, CD4 or asGM1 i.p. **i**, Representative H&E staining of brains from **h** collected on day 14 after tumor cells re-challenge. **j**, Representative flow cytometry plots and graph showing ratio of $CD69^+CD103^+$ T cells, $CD69^+CD103^-$ T cells and $CD69^+CD62L^-$ T cells in brain and PB of T-αFgl2–treated survivors (*n* = 5), **$P < 0.01$, two-way *t*-test. **g**, Representative flow cytometry plots and graphs showing CD69 and CD103 expression on $CD8^+$ T cells in the brain and PB of T-αFGL2–treated survivors (*n* = 3~4). ***$P < 0.001$, ****$P < 0.0001$, two-way *t*-test.

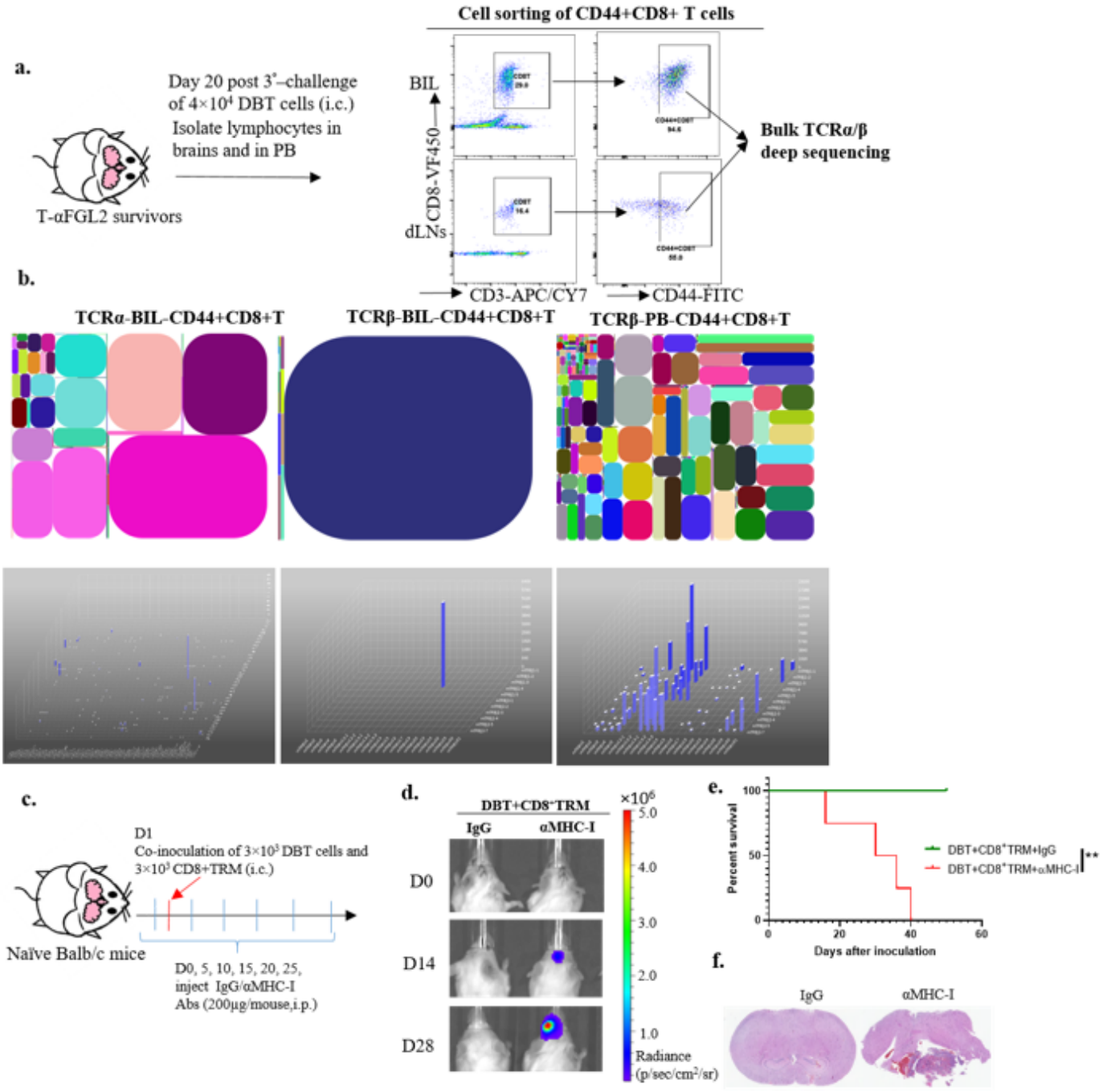

Figure 5

T_{RM} cells showed an expanded TCR repertoire.

a, Schematic of TCRα/β deep sequencing of $CD8^+$ T cells from the brains and dLNs of T-αFGL2–treated survivors. Cells were sorted via flow cytometry on day 20 after the third challenge with intracranially (i.c.) injected DBT tumor cells. **b**, Representative tree maps (top row) of TCRα-T_{RM}-$CD8^+$T, TCRβ -T_{RM}-$CD8^+$T, TCRβ-dLNs-$CD8^+$T clones. Each spot represents a unique entry: V-J-CDR3, and the size of a spot denotes its relative frequency; 3D map of V and J usage of TCRα-T_{RM}-$CD8^+$T, TCRβ-T_{RM}-$CD8^+$T, TCRβ-dLNs-$CD8^+$T clones (bottom row). **c**, Schematic of experimental design. Day 1, 3 × 10^4 $CD8^+T_{RM}$ cells and 3 ×

10^3 DBT cells were coinoculated i.c. into the naïve Balb/c mice; day 0, 5, 10, 15, 20, and day 25 the mice were treated with IgG or MHC-I blocking antibodies (100μg/mouse,i.p.). **d**, Representative bioluminescence images of Balb/c mice on days 0 and 14 and day 28 after i.c. transplantion with $CD8^+T_{RM}$ and DBT cells. **e**, Kaplan-Meier survival curves of mice in **f** (n = 4 mice/group). *p = 0.0101, log-rank test. **f**, Representative H&E staining of brains from **d** collected on day 40 after transplantation.

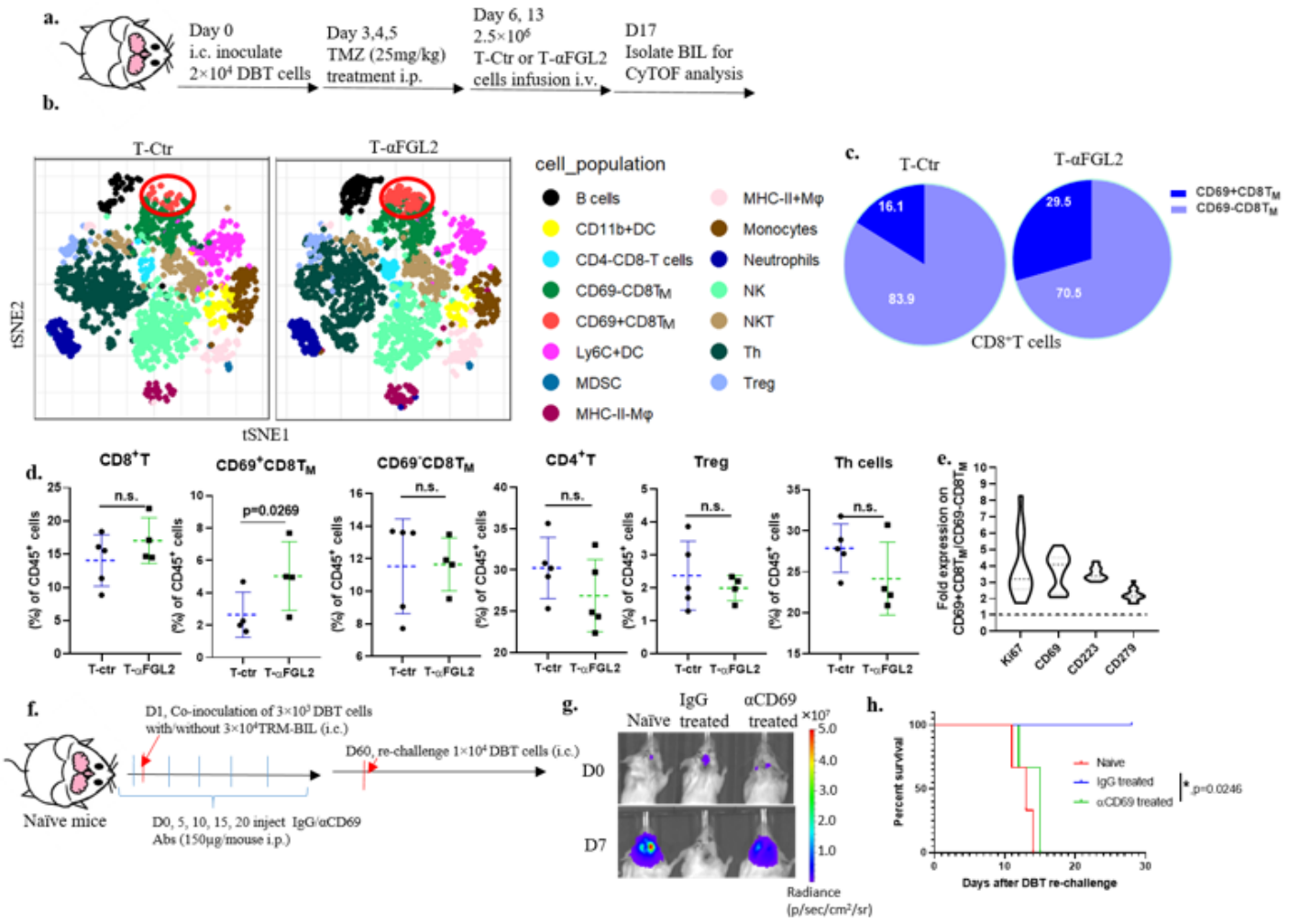

Figure 6

T-aFGL2 treatment increased the $CD69^+CD8^+T_M$ cell subset.

a, Schematic of the experimental design. Four days after infusion of T-Ctr or T-αFGL2, brains were collected to isolate brain-infiltrating lymphocytes (BIL), which were then stained with antibodies conjugated to metal isotopes. Mass cytometry (CyTOF) single-cell data was clustered to identify common populations across the treatment groups. **b**, T-distributed stochastic neighbor embedding (tSNE) analysis of $CD45^+$ cells from the brain, colored by relative expression of CyTOF markers. Cell populations are indicated on the right. **c**, Composition of the $CD8^+$ T cell compartment in T-Ctr and T-αFGL2–treated DBT-bearing mice showing increased frequency of $CD69^+CD8^+$ T_M cells in the brains of T-αFGL2–treated mice.

d, Frequencies of total $CD8^+$ T cell population and subsets of $CD8^+$ T cells and $CD4^+$ T cells (*n* = 4-5 mice per group). **e**, Fold expression of Ki67, CD69, CD223, and CD279 on the $CD69^+CD8^+T_M$ subset and the $CD69^-CD8^+T_{EM}$ subset. **f**, Schematic of experimental design. Day 1, 3×10^4 $CD8^+T_{RM}$ cells and 3×10^3 DBT cells were coinoculated i.c. into the naïve Balb/c mice; day 0, 5, 10, 15, and day 20, the mice were treated with either IgG or CD69 blocking antibodies (150ug/mouse i.p.); day 60, Balb/c mice bearing transplanted $CD8^+T_{RM}$ were re-challenged with 1×104 DBT cells (i.c.). **g**, Representative bioluminescence images of Balb/c mice on days 0 and 7 after i.c. re-challenge with DBT cells in **f**. Data are representative of two independent experiments. **h**, Kaplan-Meier survival curves of mice in **f** (*n* = 3~4 mice/group),log-rank test.

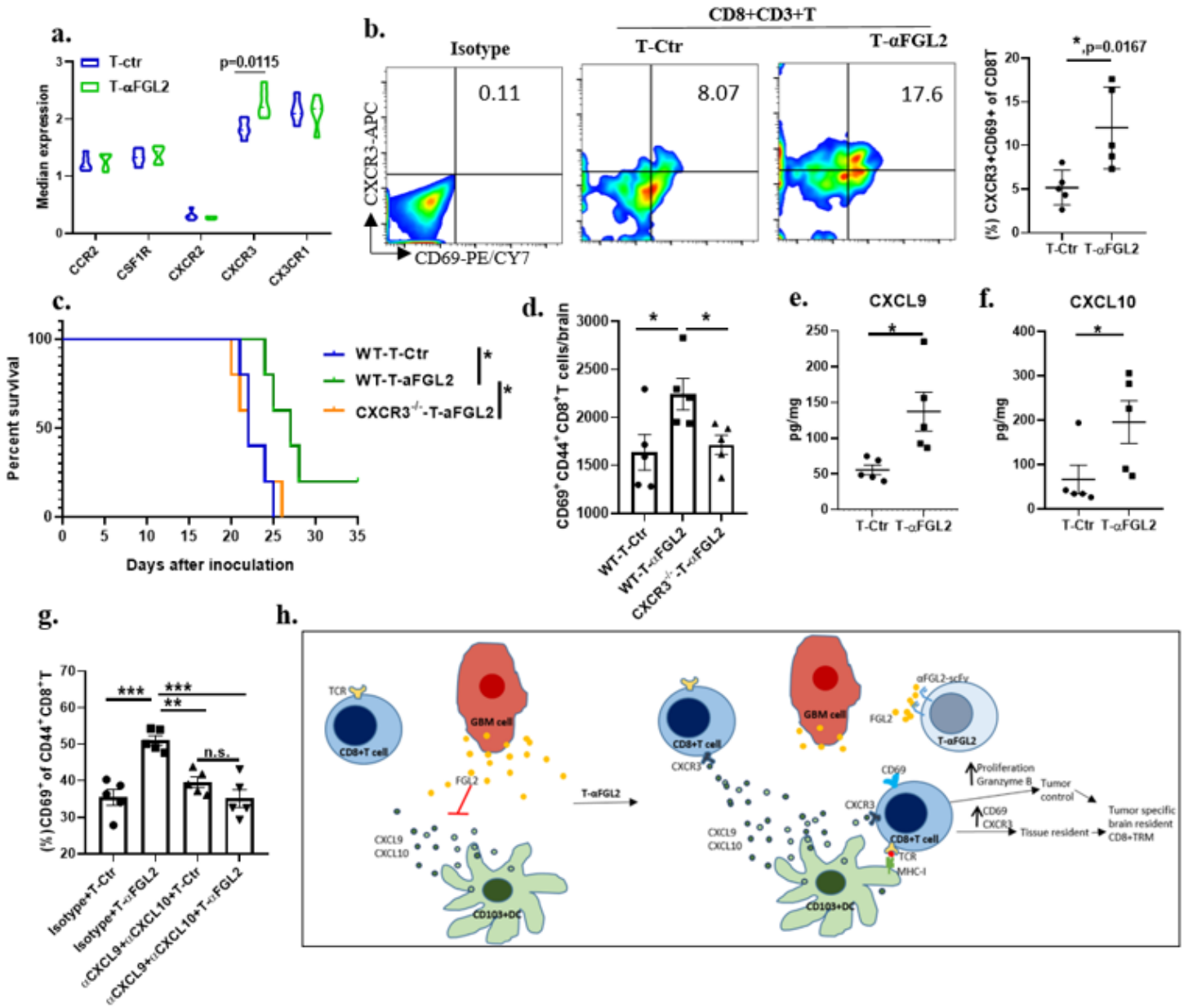

Figure 7

T-aFGL2 induced $CD69^+CD8^+T_M$ was associated with CXCL9/10-CXCR3 axis

a, Quantitative expression level of CCR2, CSF1R, CXCR2, CXCR3,and CX3CR1 on $CD69^+CD8^+T_M$ populations of T-Ctr and T-aFGL2 group from CYTOF data. **b**, Representative flow cytometry plots and graphs showing T-aFGL2 treatment increased $CXCR3^+CD69^+CD8^+$T cells among total $CD8^+$T cells in glioma bearing brains. **c**, Kaplan-Meier survival curves of GL261-bearing wild-type mice (WT) and CXCR3 deficient mice ($CXCR3^{-/-}$) treated with T-Ctr or T-aFGL2 (*n* = 5 mice/group). **P* <0.05, log-rank test. **d**, Quantitative data showing $CD69^+CD8^+T_M$ cells number per GL261-bearing brain on day 5~7 post 2^{nd} T cells therapy. **P* <0.05, two-way *t*-test. **e**, Quantitative protein analysis of CXCL9 and CXCL10 in DBT tumors from mice 4~6 days after 2^{nd} therapy of T-Ctr or T-aFGL2. Data represent the mean ± SEM; *p < 0.05, two-way t test. **f**, Kaplan-Meier survival curves of DBT-bearing Balb/c mice treated with T-Ctr or T-aFGL2, combined with isotype control or anti-CXCL9 and anti-CXCL10 antibodies (n=5 per group). *p<0.05, log-rank test. **g**, Percentages of CD69+ out of CD44+CD8+T cells. Data represent the mean ± SEM; **p < 0.01, ***p<0.001, one-way ANOVA with Tukey's multiple comparison test. **h**, Schematic illustration of cellular and molecular events underlying T-aFGL2 induced tumor specific brain resident $CD8^+T_{RM}$. T-aFGL2 cells block the FGL2 in the tumor microenvironment, resulting in $CD69^+CD8^+$T cells population enrichment and CXCL9/10 induction. These CD69+CD8+T cells were boosted through CXCL9/10-CXCR3 engagement. The $CXCR3^+CD69^+CD8^+$T cells are candidate of tumor specific brain resident $CD8^+T_{RM}$ as these cells show both TRM phenotype ($CD44^+CD69^+CD62L^-$), and proliferative activity ($Ki67^+$) inside the brain tumors.

Supplementary Files

This is a list of supplementary files associated with this preprint. Click to download.

- SupplementarydataMethodandMaterialsV6.docx